Heritage Science

RESEARCH

Open Access

3D digital technologies applied to the design and printing of auxiliary structures for fragment adhesion strategies on wax artifacts

Emanuel Sterp Moga[1*], Óscar Hernández-Muñoz[2], Javier del Río Esteban[3] and Alicia Sánchez-Ortiz[1]

Abstract

Three-dimensional models of anatomy in wax preserved in university museums are rare artifacts of extraordinary technical complexity. In recent years, interest in them has increased among scholars who consider them primary sources of heritage value to approach material culture and the history of science. The fragility of the sculptural material and the inadequate exhibition and storage conditions of many of these collections have caused the formation of pathologies whose conservation treatment is a great challenge for the restorer. In this regard, new 3D digital technologies have created a great impact on the documentation and analysis of interventions in the field of conservation and restoration of cultural heritage. This research aims to demonstrate the technical possibilities offered by 3D digital systems as support tools in curative conservation strategies to mechanically stabilize fragmented sculptural parts. For this case study, we chose an 18th-century obstetric anatomical model made by the Madrid Court sculptor Juan Cháez, and the modeler Luigi Franceschi who belonged to the anatomical cabinet of the Royal College of Surgery of San Carlos in Madrid. In this work, we demonstrate the digitization process carried out employing structured light scanners, digital modeling, and 3D printing. The aim is to create auxiliary structures suitable to support the various original pieces to be adhered while guaranteeing their exact position during the adhesive curing process as well as the volumetric reintegration of faults. In addition tensile and three point bending tests for the mechanical characterization of the selected thermoplastic impression materials are described. Finally, the qualities considered suitable for the most appropriate material for the purpose of the study are detailed. Promising results were obtained since the structures have made it possible to perform fragment adhesions in highly complex areas of the sculpture, ensuring maximum precision, safety, and efficiency during the process.

Keywords: 3D scanning, 3D printing, Mechanical properties, Tensile tests, Flexure tests, Thermoplastic materials, Auxiliary structures, Wax sculpture, Conservation-restoration, Adhesion of fragments

Introduction

The elaboration of three-dimensional wax models was one of the main objectives of the Royal College of Surgery of San Carlos during the eighteenth century. The set of sculptures they produced significantly contributed to the reputation of the institution and helped the advancement of health sciences within the educational project defined during the Enlightenment period.

*Correspondence: emasterp@ucm.es

[1] Department of Painting and Conservation-Restoration, Faculty of Fine Arts, Complutense University of Madrid, C/ Pintor el Greco, 2. Ciudad Universitaria s/n, 28040 Madrid, Spain
Full list of author information is available at the end of the article

Wax occupied a unique and privileged place in the art of representing the human form. Its ability to emulate the translucency of the skin made it an ideal medium for the creation of realistic sculptures, both in the representation of internal structures and their external appearance. By combining it with other materials (human hair, bones, fabrics…), the sculptor was able to create a version of the body that was disturbing in its mimetism.

As the eighteenth century saw advances in the study of anatomy and pathology, this technology was harnessed to create durable and realistic three-dimensional models of the most recent discoveries. The most important universities of the time developed their own wax modeling workshops, although the most famous ones were established in the cities of Florence, Bologna and Vienna. The ceroplastics sculptors who worked in these anatomical cabinets carried out their work in close collaboration with the anatomists with the purpose of constructing polychrome wax models that could serve as didactic material, substitute of the real specimen, during the practical explanations in the classrooms. The physical interaction with the models allowed students a deeper understanding of anatomy in accordance with the educational trend of the time that recognized the advantages of physical learning.

The technical procedures used in the art of ceroplastics varied from one school to another, as each wax sculptor developed his own technique, which he perfected and modified over time, and which as a craftsman-artist he guarded with great suspicion, which has hindered knowledge about issues related to the ingredients of the pastes, such as the combination and proportions of each ingredient. A detailed description of the functioning of the anatomical cabinet of the Royal College of Surgery of San Carlos is available in Bonells y Lacaba's book Curso completo de anatomía del cuerpo humano, published in 1800, being especially interesting the last section of book V, dedicated to the art of working anatomical pieces in wax [1].

In general terms, once the anatomical dissector had prepared the specimen to be reproduced, a copy of it was made with chalk or wax and on this the plaster molds were made, which would serve as a matrix to reproduce the same model as many times as desired. The main component of the modeling pastes was beeswax or virgin wax, to which other substances were added, such as natural resins, Venice turpentine or purified common turpentine, a low-quality substitute, and animal or vegetable fats, lard without impurities, which made it possible to modify the melting point and make them more suitable for sculptural purposes. Pigments, finely ground and agglutinated with turpentine, or colorants could be added to the melted waxy paste to imitate the chromatic qualities of each anatomical part to be represented. In the Madrid cabinet, fine carmine, vermilion and superfine lacquer were used to imitate the living muscle, vermilion for the arteries, Prussian blue for the veins, white lead to imitate nerves, ligaments and absorbing vessels, and red lacquer with a little white to imitate the rosy skin. Inside the molds, the more or less fluid wax was poured in layers of varying thickness, in order to obtain the desired consistency. Once the mold was opened and the positive was extracted, the last phase consisted of applying the final details with the imitation of textures and striations in the muscles or the placement of lymphatic vessels, veins, arteries and nerves, which were done by embedding silk threads in the colored wax pastes. Once this work was concluded, a thin film of transparent varnish was applied to obtain a finish in accordance with the natural one [2].

The anatomical wax collections represent scientific rigor with great delicacy in the artistic representation of the figures. Exhibited in contemporary showcases with minimal interior space many of the models rub against each other which makes it difficult to handle. This entails a higher risk during its movement. Some of the sculptures show losses or have fragmented elements like mechanical damage due to accidental blows that sometimes cause serious integrity problems. In extreme situations, this can compromise the future preservation of the object [3]. Due to the particular fragility of the waxy material chosen for sculptural support, the traditional procedures used for the adhesion of detached fragments usually present some technical difficulties to the restorer. This is because it is not possible to exert direct pressure on the areas to be joined and also because it is essential to keep the pieces level and stable until the adhesive has completely cured and the volumetric reintegration is complete.

In recent years, 3D digital systems based on scanning, modeling, and 3D printing have become tools with enormous potential for documenting, diagnosing, preserving, and disseminating cultural heritage [4–10]. In particular, 3D printing has played an increasingly relevant role in the field of conservation-restoration. Also, different applications have shown great potential, offering new alternatives for analysis and intervention. Because of this, it has been possible to considerably reduce manipulations on the item, adequately plan each treatment, and reproduce additional or missing elements to complement various restorations. This is all possible while ensuring maximum respect and minimum intervention upon the work [11–13]. Throughout the course of 3D printing, several factors influence the manufacturing process regarding the mechanical characteristics of the object. Among these are the position, orientation angle, and infill density that is, the grid pattern that the printing software creates

to partially fill the inside of a part in order to give it more strength. Such characteristics have been analyzed by several researchers in the most common FDM (Fused Deposition Modeling) additive printing materials such as PLA, ABS, or PET, while also highlighting their importance [14–17].

One of the main aspects to be considered when printing is the anisotropy of the parts created due to the construction technology. Anisotropy is the tendency of a material to show changes in its physical properties when arranged in different orientations [18]. Although many 3D printed materials are isotropic, which means they do not change their properties when their orientation changes, printed parts will show anisotropy in their physical properties due to the layering process by which they are constructed. Material extrusion 3D printers based on fused deposition modeling FDM technology are the most common type of equipment used in 3D printing [19]. They are based on a process by which a polymer filament is extruded and deposited in layers to create a 3D object [20]. As a result of layered deposition, the object created by this process has an anisotropic character. The orientation of the layers determines, for example, a higher bending strength in a particular direction compared to others.

Research aim

In this article, we present a new method for dealing with complex situations centered on the structural consolidation of fragment adhesion in wax sculptures. Specifically, we propose the scanning of the work in order to obtain a virtual model on which to design various auxiliary structures. Once obtained by FDM additive printing, it makes it easier for the restorer to operate with guarantees of safety and precision during the process of handling, leveling, and adhesion of the damaged pieces to recompose the whole sculpture. In order to ensure the maximum efficiency and safety of the 3D printed structures that will support the fragments to be bonded, different manufacturing morphologies have been analyzed as well as the mechanical properties of a wider range of thermoplastic materials utilizing standard tensile and bending tests.

State of conservation of the anatomical model

This case study is a polychrome wax sculpture, round and hollow, with dimensions of $22 \times 44 \times 56$ cm, conserved in the Javier Puerta Anatomy Museum and inventoried under the name of Internal version (Ref. MOSP 000328). It was created by the sculptor Juan Cháez and the wax modeler Luigi Franceschi (Fig. 1). The figure shows the interior of the pelvic cavity with the anterior aspect of the uterus sectioned to show the fetus while the obstetrician's hands reposition it by manipulating its extremities in order to extract it.

Fig. 1 Internal version. © Luis Castelo

As a result of its original didactic function, the sculpture has been subjected to frequent and repeated manipulations that have conditioned its current state of conservation. As a result of the constant use of the object by students who followed the anatomist's explanations, a series of mechanical degradations have been located primarily in the protruding parts of the work (hand, fingers and foot). This situation has compromised the original meaning of the artifact.

Besides the anthropogenic factor, which is considered the main cause of deterioration, there are other intrinsic and extrinsic factors. As time has passed, the wax pastes of the eighteenth century used in the preparation of the model have undergone natural aging. This has led to a series of physical–chemical changes in their internal structure, which at the same time has become a much more brittle material. In addition to the natural aging of the wax itself, other causes such as fluctuations in relative humidity and temperature have also contributed to the origin of fissures and cracks in the most vulnerable parts. This is due to the constant changes in contraction and expansion that the material has undergone in response to climate conditions (Fig. 2) [21, 22]. Greatly enhanced by the multiple manipulations mentioned above, several fractures and the loss of some elements including the middle finger have occurred. These factors, along with the neglect suffered due to changes in teaching methods, have been lethal for the work [3].

During the diagnosis of each of the fragments to be adhered, several difficulties were encountered when trying to approach the intervention with precision. Several elements did not have the same joining surface, making it very difficult to locate each one of them in its original place. Therefore, it was considered necessary to virtually analyze the necessary treatments and to print the

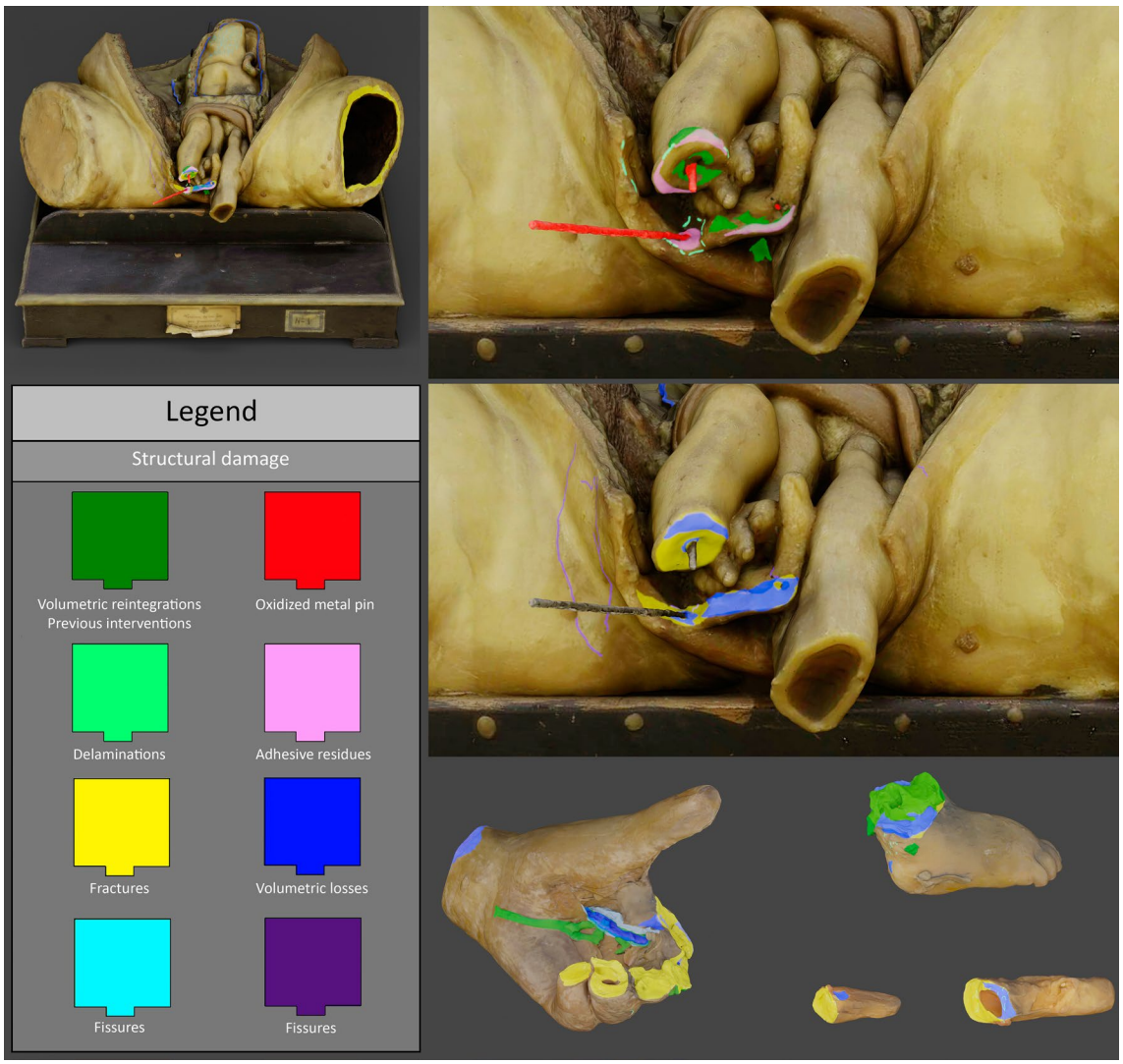

Fig. 2 3D mapping of structural pathologies

different auxiliary structures to guarantee the stability of the fragments during the intervention process.

Materials and methods

Digitizing using structured light scanners

Aiming to have a virtual model faithful to the real object and achieve the highest possible quality in the polygon mesh, the sculpture was digitized using a combination of two structured light 3D scanners. These were: the Space Spider model and the Eva model (Artec 3D, Luxembourg City, Luxembourg). The first device had a 3D point accuracy, up to 0.05 mm and a 3D resolution of 0.1 mm and the second had a 3D point accuracy, up to 0.1 mm and a 3D resolution of 0.2 mm. These results are adequate for the requirements of the study proposed in this work. Two strategies were used to carry out the volumetric recording. The first consisted of keeping the anatomical model static and surrounding it from different points of view. This tactic was used only to scan the entire work given its dimensions. The second strategy focused on placing the object on a rotating platform to facilitate the scanner's sweep from different orientations. This method was used mainly to digitize the smallest fragments of the damaged elements. A combination of both scanners was used in the same session to record the complete volume with high definition. First, the entire figure was scanned with Artec Eva and then the areas of greater anatomical detail were captured with Artec Space Spider.

The processing of the scanned data was performed using Artec Studio Professional 15 software (Artec 3D,

Luxembourg City, Luxembourg). This consisted of repositioning and aligning the different scanned fragments of the model. First, we examined all captured frames containing the spatial and chromatic information of the object and removed those with errors or poor quality to increase accuracy during data processing. Next, we ran the global registration tool, which analyses the position in space of each point captured by the scanner and unifies all the equivalent points from the different frames into a single point cloud. The 3D noise was filtered to remove all the small areas not connected to the main mesh because they could create irregularities on the surface of the model. In order to obtain the high-resolution polygonal mesh, we use the hard fusion option, since it is the one that achieves the highest definition. Finally, the two models generated with Artec Eva and Artec Space Spider were merged.

Fragment composition analysis by virtual anastylosis

All the meshes of the digitized fragments were imported into ZBrush 2020 (Pixologic, Los Angeles, California, USA), where they were repositioned to fit together using the available transformation tools. After this process, it was observed that the middle finger of the obstetrician's left hand, which grasped one of the fetus' legs, had disappeared. However, it was possible to deduce its position from the location and orientation of the adjoining fingers. This finger was also modeled in ZBrush and placed in its corresponding location.

3D modeling of auxiliary structures

Once the scanned models were obtained in the 3D computer graphics software Blender (Blender Foundation, Amsterdam, The Netherlands), we proceeded to design each part from different cubes, spheres, and cylinders. Tools such as *bevel*, *loop cut*, or *knife* were used to facilitate the modeling. In order to obtain maximum precision in the parts with the most complex shapes and to achieve a correct fit between them, the *boolean* tool was used. Multiple combined operations of union, subtraction, and intersection were performed to achieve the desired results.

During the virtual modeling of the auxiliary structures, the digitized model has been used at all times to compare the accuracy, efficiency, and all the structural details required in each case. At the same time, during the design process we paid attention to the functionality of the delicate and waxy material and its compatability with the fragments. Finally, we also took into consideration the arrangement of fractures and cracks in the material to make sure that sufficient stability, strength, and toughness were taken into account.

Mechanical testing of thermoplastic materials for 3D printing of auxiliary structures

Aiming to identify the most appropriate material and fabrication morphology for the auxiliary structures that will support the fragments of the work, tensile and bending tests were performed with different materials and fabrication configurations. The tensile tests were carried out on a Microtest SCM 3000 95 (Microtest, Madrid, Spain) machine following the specific International Organization for Standardization standard for the testing of Plastics—Determination of tensile properties UNE-EN ISO 527-1:2020. The bending tests were performed on an Adamel Lhomargy DY30 (Adamel Lhomargy, Roissy-en-Brie, France) machine according to the specific standard for the testing of Plastics by International Organization for Standardization—Determination of flexural properties UNE-EN ISO 178:2020. Tensile tests are the most widely used studies for the characterization of material properties, but because of the configuration of supports and weights in our restoration, the structures will be subjected to bending too. Thus, it was considered relevant to perform standardized bending tests to complement and contrast the results obtained with the tensile tests.

Aiming to find the most suitable printing orientation characteristics, 45 PLA (polylactic acid) specimens were tested in which the angle was varied at 0° and 90° in the horizontal position and at 0° in the vertical position according to its longitudinal axis that forms the plane of the specimen with the printing platform (Fig. 3). With each angle, 15 specimens were created (5 with a density of 100%, 5 with a density of 50% and 5 with a density of 10%). The main objective was to find the best possible orientation and filling density for the impression of the structures.

Once we determined the best orientation and percentage of infill for PLA printing, we tested 10 other materials under the optimal manufacturing conditions previously obtained for PLA in order to choose the most suitable material for the construction of the supports. These were: ABS (acrylonitrile butadiene styrene), PETG (polyethylene terephthalate), ASA (acrylonitrile Styrene Acrylate), NYLSTRONG [nylon (PA6) Polyamide with glass fiber], HIPS (polystyrene and polybutadiene rubber), INNOVATEFIL POLYCARBONATE (polycarbonate), PP (polypropylene), PLA 3D870 (polylactic acid), INNOVATEFIL CO-POLYESTER (copolyester), and PA CF (polyamide with carbon fiber).

Each of the specimens was printed using an Ultimaker S5 (Sicnova, Linares-Jaén, Spain) machine with a resolution of 0.1 and 1.5 in wall thickness, a grid pattern, and a printing speed of 50 mm/s. The printing temperature varied between 215 °C and 270 °C and the hotbed

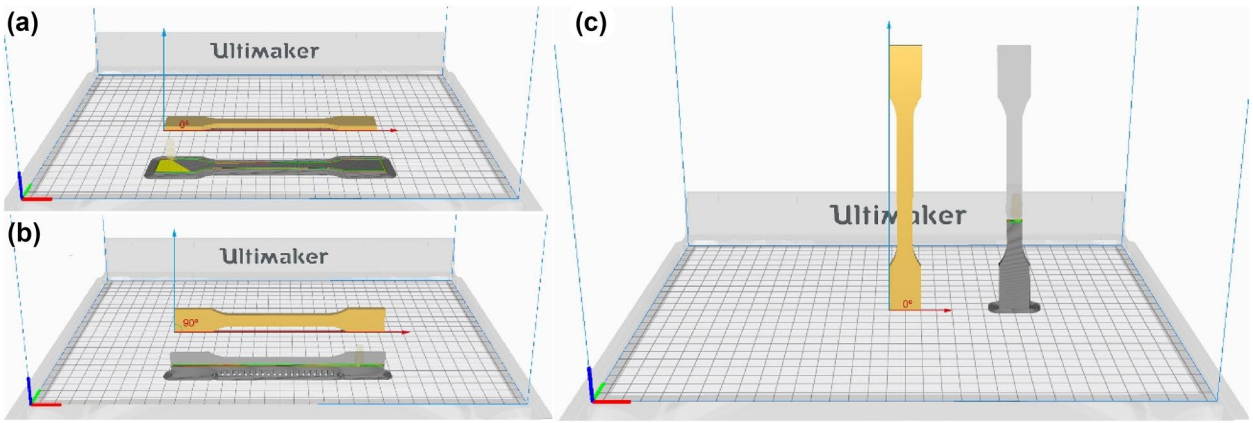

Fig. 3 Printing positions of the specimen. **a** Horizontal 0°. **b** Horizontal 90°. **c** Vertical at 0°

temperature shifted between 60 °C and 100 °C depending on each material.

3D printing of structures

The 3D printing of the auxiliary structures was carried out using the printer mentioned above. The machine features a high layer resolution of up to 20 microns (0.02 mm), a print volume of 330 × 240 × 300 mm, a print speed < 24 mm^3/s, and a filament diameter of 2.85 mm. Other features include a double extruder with 0.4 mm nozzles. The possibility of working with a water-soluble material such as PVA (polyvinyl alcohol) simultaneously with the resistant material for the figure, ensures very high quality and precision in any type of geometry. The models to be printed were imported in STL format and configured employing Cura 4.10 software (Ultimaker, Utrecht, The Netherlands). The best-performing parameters obtained in the tensile and bending tests were used for the configuration of the impression of the suxillary structures.

Results and discussion

Digitizing using structured light scanners

The anatomical model obtained after combining the Artec Eva scanner used for the general registration (Fig. 4a) and Artec Space Spider for the details and smaller fragments (Fig. 4b), made it possible to generate a high-quality model. A mesh of 15,168,150 polygons has been obtained for the entire work (Fig. 4d).

Fragment composition analysis by virtual anastylosis

All the fragments of the virtual model except the left hand of the obstetrician were placed in their correct position, adjusting quite precisely to each other and leaving hardly any space between them. This process is known as anastylosis. Once the location of the hand in its original site was established, it became clear there was a large area of missing material (Fig. 5a). Such information revealed the difficulty that would be faced when ensuring the stability of the hand during the bonding process. Another finding that was central to the stability of the adhesions as a whole was the missing middle finger. A metal bolt located in the middle phalanx of the index finger was found to cross the middle finger to provide greater consistency to the hand (Fig. 5c). Because this piece is a central element, it was decided to incorporate it to ensure the stability of the adhesion set. Regarding the fetal foot and the fingers of the obstetrician's left hand, certain difficulties were also detected when making the adhesion. These were due to the irregularity of the joining surfaces (Fig. 5b and d). The problems encountered at various points during the adhesion and volumetric reintegration processes led to the meticulous study and modeling of the auxiliary structures to stabilize each of the fragments accurately and safely.

3D modeling of structures

3D modeling along with *bevel*, *loop cut*, and *knife* tools have made possible the restoration of quite complex numerous parts (Fig. 6a–c). The *boolean* has been one of the most effective tools when designing of the figures because its options of *substraction*, *union*, and *intersection* we have achieved a high precision modeling in very complex parts. This has allowed a perfect fit of each of the components that make up the auxiliary structure. In addition, we have created auxiliary structures that are adapted to a very precise scale on the corresponding fragments, thus ensuring great stability during the intervention (Fig. 6d–f). The result of the virtual anastylosis has been key since each structure and the operative methodology have been specifically designed according to the position of each fragment.

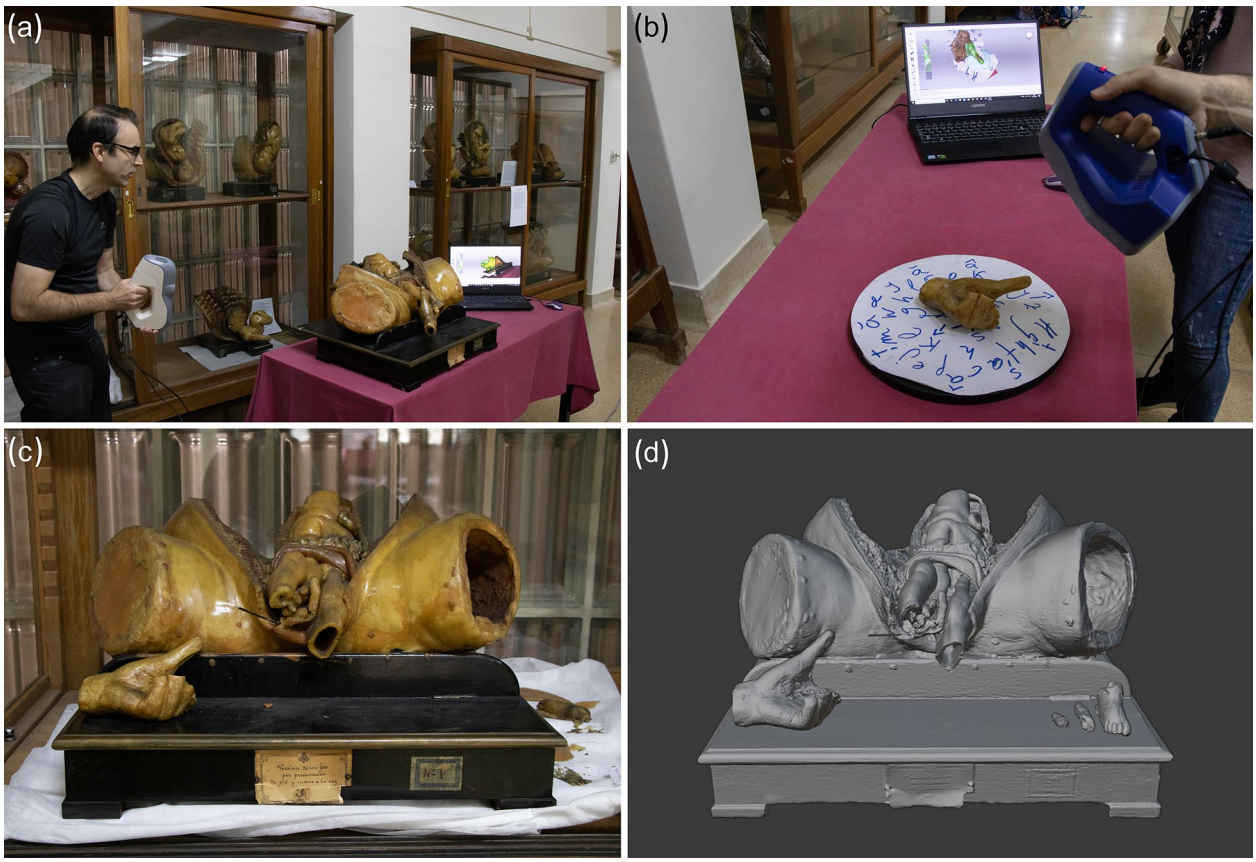

Fig. 4 Scanning process and obtaining the model. **a** Artec Eva scanning process rotating around the work. **b** Artec Space Spider scanning process rotating the fragments using the rotating platform. **c** Original model. **d** Processed virtual model

In our case study, two types of auxiliary structures were finally obtained. The first is focused on holding fragments such as the foot and fingers of the obstetrician's left hand (Fig. 7a). Each structure is made up of a base that allows the brackets that support the spheres to be housed inside. The clamps are closed by pressing the sphere inside employing the screws and nuts located on the upper part. The spheres have a hole that allows the placement of different masts which in turn are joined with another clamp system with a double sphere. The use of this last system was decisive in achieving a greater margin of movements and angles. The upper sphere of the double clamp has another hole that allows the attachment of different masts with various dimensions, as well as a wide variety of heads equipped with elastic straps to stabilize the toes and an auxiliary structure that adapts to the surface of the foot.

The second structure is designed for the adhesion of damaged fragments that compose the shape of the hand (Fig. 7b). It has a base with four cavities in the central part to accommodate different pillars that support the base of the clamp. This base has a threaded hole in the central part to insert a screw that allows the clamp to be manipulated upwards and downwards. There are two pillars located on the sides that work as guides during the millimetric lifting of the system. Similar to the case discussed before, the clamp has a sphere inside that is tightened by means of the system of screws and nuts located in the upper part of it. Finally, it also has a hole that allows the attachment of the head that supports the hand auxiliary structure.

Once the structures were completed, different virtual simulations adopting different positions were conducted to confirm their functionality and efficiency. This allowed us to calculate the most appropriate spaces and maneuvers for the intervention (Fig. 7c).

The auxiliary supports helped to hold all these delicate and fragile parts firmly, precisely and securely in place. Performing such operations to achieve maximum precision using conventional tools would be very difficult indeed. 3D modeling is the way forward for perfecting intervention techniques for complex fragment adhesions.

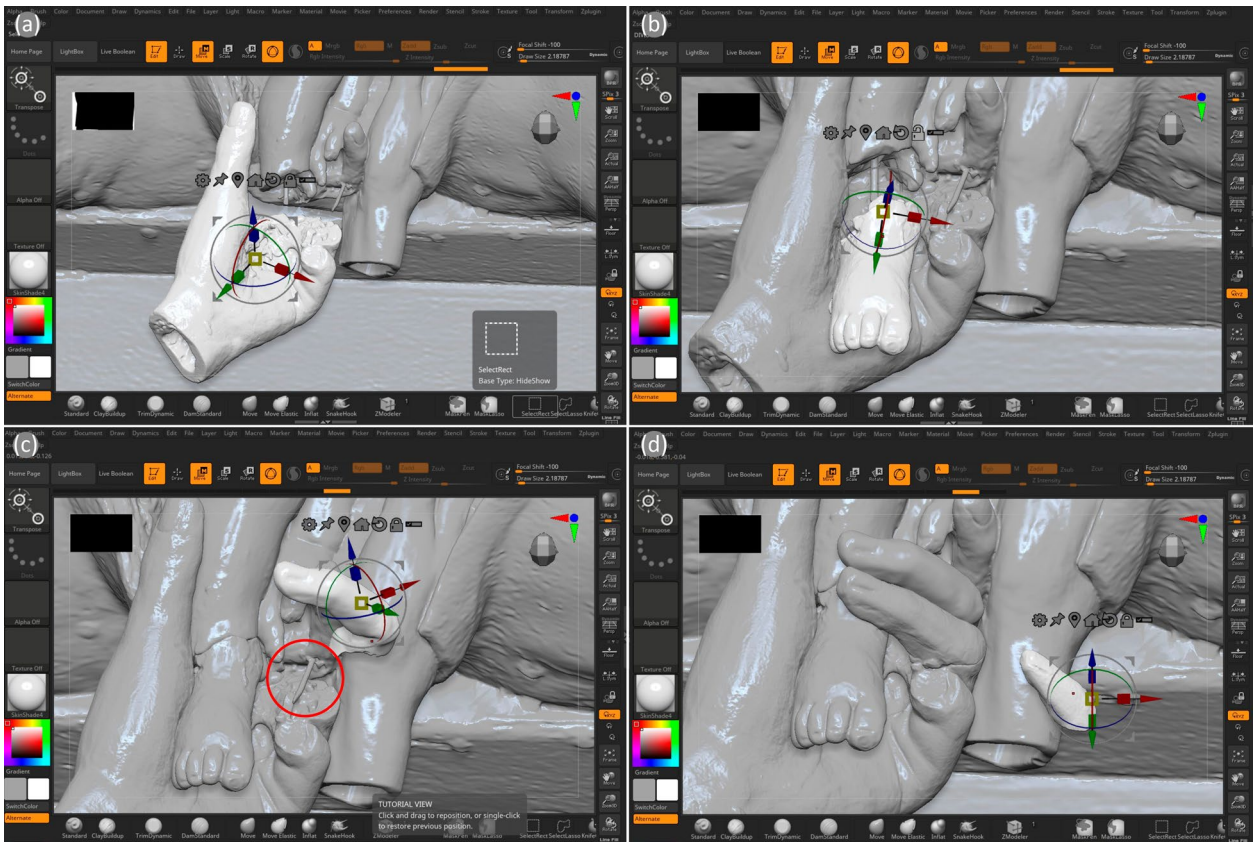

Fig. 5 Virtual anastylosis process. **a** Process of placement of the obstetrician's left hand. **b** Process of placement of the fetal foot. **c** Process of placement of the middle finger. In the marked circle, the metal bolt that would go through the middle finger can be seen. **d** Process of positioning the little finger

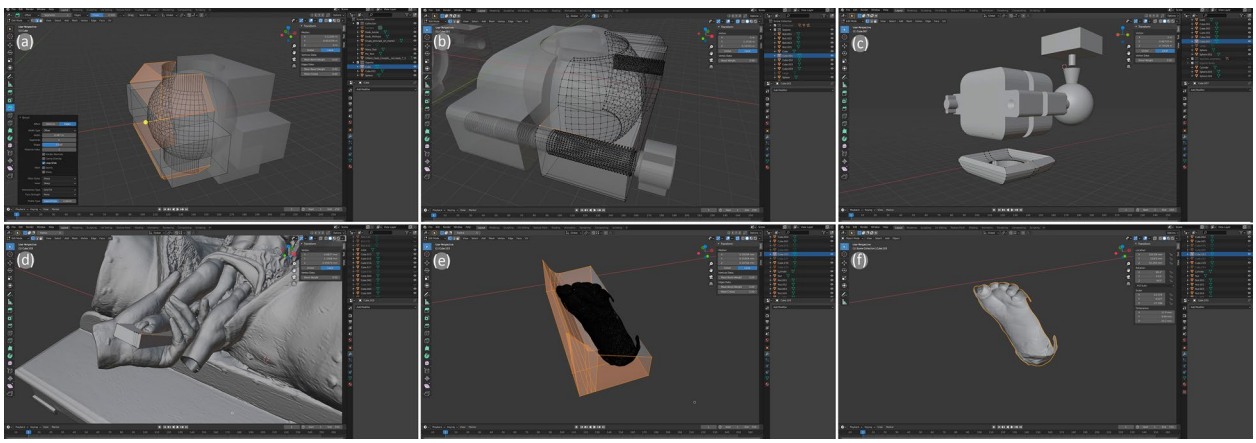

Fig. 6 **a**–**c** Modeling process of the structural parts. **d**–**f** Modeling process of the the auxiliary structure of the foot

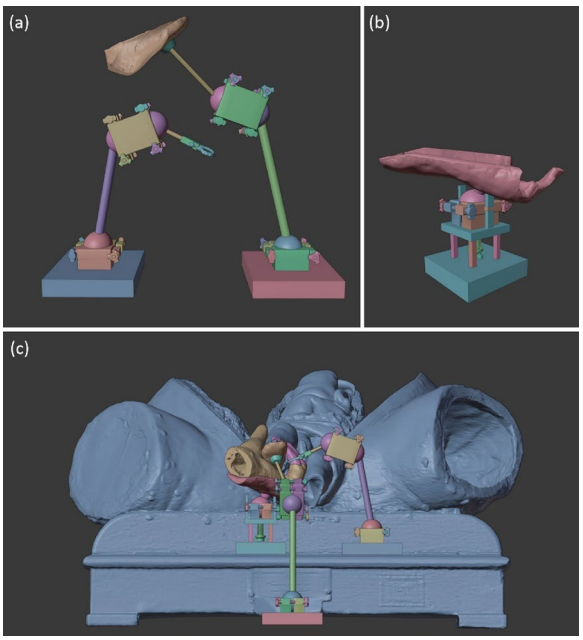

Fig. 7 **a** and **b** Composition of the different elements that make up the auxiliary structure. **c** Application and testing of the auxiliary structures during fragment adhesion

Mechanical testing of thermoplastic materials for 3D printing of ancillary structures

Tensile tests: analysis of the geometry construction and filling density of specimens

In order to analyse the influence of printing orientation of specimen, several specimen of PLA have been built in the configuration described above. In Table 1 we present the mechanical parameters for every manufacturing morphologies of PLA specimens. For comparison, in Fig. 8, the nominal stress-nominal strain curves for different configurations are shown. As can be seen from the results collected in Table 1 both, position and filling density play a determining role in the mechanical performance of the specimens.

In Fig. 9 the dependence of the tensile modulu and yield strength versus filling density have been shown. As can be seen, tensile modulus increased with filling density, that is, the strength of specimen is bigger the bigger is filling density. However, while a geometry of vertical position at 0° (VER 0°) produced specimens with a very low strength, no significant differences between the horizontal position at 0° and 90° (HOR 0° and HOR 90°) were observed. A similar behavior is observed for yield strength in reference to filling density and geometry of specimen (Fig. 9b).

The vertical position at 0° turned out to be the weakest because it has the lowest modulus of elasticity and yield strength for all densities. However, the infill density improves the mechanical properties of the specimen, increasing both, elastic modulus and yield strength in 50% when specimen are filling from 10 to 100%. In the case of printing angle, it is noticeable that the mechanical properties of specimens manufactured at 90° are slightly higher than those at 0°. Therefore, based on these initial results, the different selected materials have been analyzed in the horizontal position at 90°.

Tensile tests: analysis of different thermoplastic materials

In Table 2 we present the mechanical property parameters of the 11 materials tested on specimens built in the horizontal position with a 100% filling density. In Fig. 10 we show their nominal stress-nominal strain curves. Results show that the PA CF is the material with the highest values of modulus and yield strength and therefore, the ideal material to produce the auxiliary structures. However, as a consequence of the presence of carbon fiber, its printing process is complex and

Table 1 Tensile test results

Specimens	Printing material	Orientation	Filling density (%)	Printing time per specimen	Tensile modulus of elasticity [MPa]	Yield strength σ0.2% [MPa]	Strain at yield strength σ0.2%	Tensile stress [MPa]
PH10	PLA Polylactic acid	Horizontal 0°	10	109 min	1305	32	0.028	38
PH50	PLA Polylactic acid	Horizontal 0°	50	117 min	1450	36	0.028	44
PH100	PLA Polylactic acid	Horizontal 0°	100	172 min	1944	49	0.028	62
PHC10	PLA Polylactic acid	Horizontal 90°	10	169 min	1392	34	0.028	38
PHC50	PLA Polylactic acid	Horizontal 90°	50	180 min	1412	32	0.026	36
PHC100	PLA Polylactic acid	Horizontal 90°	100	259 min	2066	52	0.028	62
PV10	PLA Polylactic acid	Vertical 0°	10	161 min	544	23	0.047	28
PV50	PLA Polylactic acid	Vertical 0°	50	168 min	740	25	0.035	27
PV100	PLA Polylactic acid	Vertical 0°	100	258 min	802	19	0.020	46

Mechanical parameters of each of the specimens (the strain at the yield strength is the deformation of the specimen when the applied stress has the value of the yield strength stress)

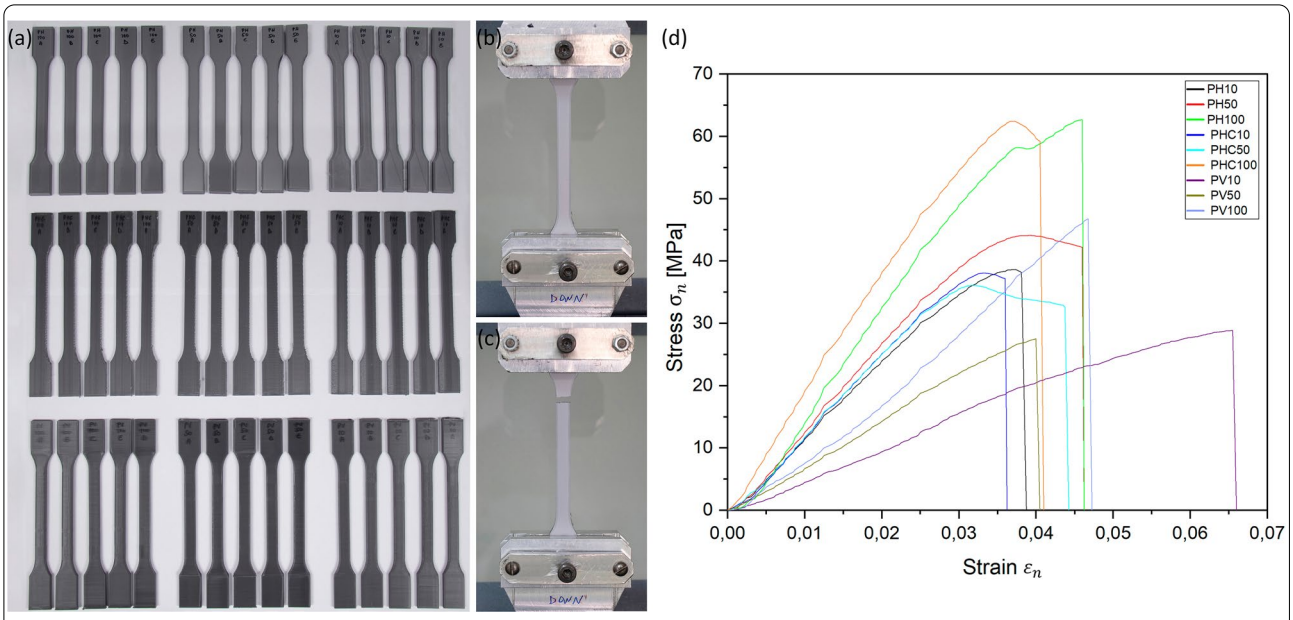

Fig. 8 **a** Tensile specimens of different PLA positions and densities. **b** Before performing tensile tests. **c** After performing the tensile test. **d** Comparison of nominal stress $\sigma_n = \frac{F}{A}$ nominal strain $\varepsilon_n = \frac{\Delta L_0}{L_0}$ curves of printed specimens for different positions and densities

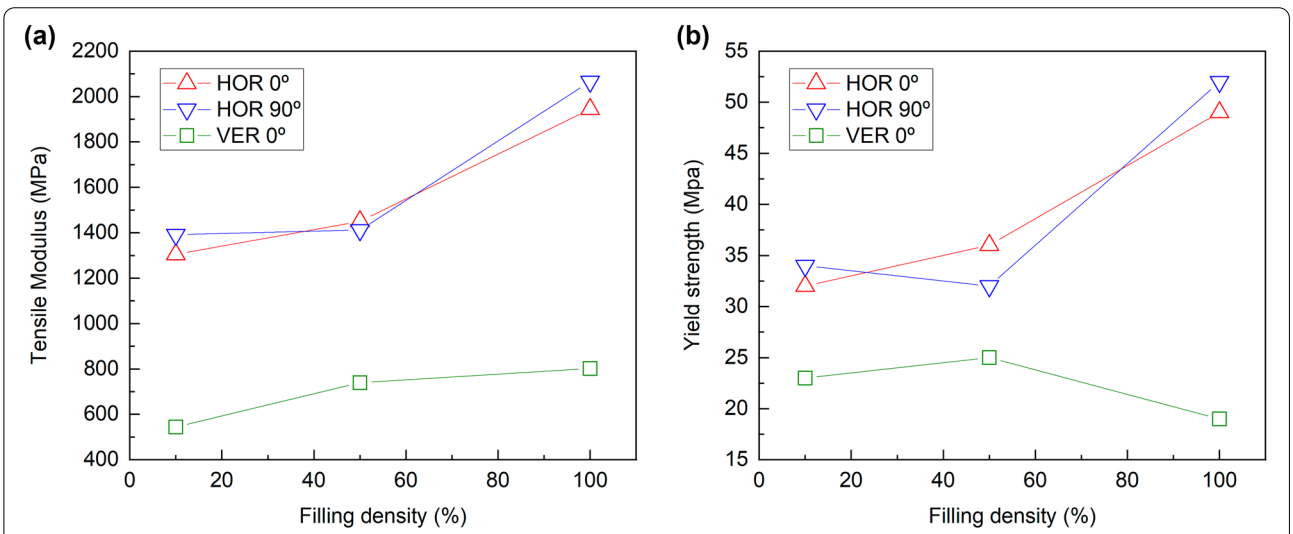

Fig. 9 **a** Relationship of tensile modulus and filler density of specimens with different positions. **b** Relationship between yield strength and fill density of specimens with different positions

cumbersome. This causes successive failures when the filament is not correctly extruded, sometimes completely clogging the brass nozzle. The latter, along with the fact that its mechanical properties are too high for the proposed purpose, makes us decide not to consider it during the manufacture of the auxiliary structures.

The second material with the highest mechanical properties was PLA. It has an elastic modulus of approximately 2060 MPa and a yield strength of 52 MPa. In addition, it is easy to manufacture and it has an optimum performance, making it the ideal candidate for the needs in the manufacture of structures. Moreover, PLA's biodegradable characteristics makes it an environmentally friendly material. The tensile strength, that is, the maximum stress that the material could withstand before the first signs of fracture appear, is 62 MPa. This would be equivalent to a load of 625 kg/cm^2, which is much higher

Table 2 Tensile test results

Specimens	Printing material	Orientation	Filling density (%)	Printing time per specimen	Tensile modulus of elasticity [MPa]	Yield strength σ0.2% [MPa]	Strain at yield strength σ0.2%	Tensile stress [MPa]
ABS	ABS Acrylonitrile Butadiene Styrene	Horizontal 90°	100	280 min	1437	37	0.032	45
PL3	PLA 3D870 Polylactic acid	Horizontal 90°	100	259 min	1730	40	0.030	54
PET	PETG Polyethylene Terephthalate	Horizontal 90°	100	259 min	1223	40	0.049	51
ASA	ASA Acrylonitrile Styrene Acrylate	Horizontal 90°	100	259 min	1238	34	0.041	46
PP	PP Polypropylene	Horizontal 90°	100	223 min	379	9	0.046	16
HIP	HIPS Polystyrene and Polybutadiene Rubber	Horizontal 90°	100	259 min	1036	17	0.017	18
NYL	NYLSTRONG Nylon [PA6] Polyamide With Glass Fiber	Horizontal 90°	100	259 min	1726	28	0.026	52
COP	INNOVATEFIL CO-POLYESTER Copolyester	Horizontal 90°	100	259 min	1443	16	0.014	25
POL	INNOVATEFIL POLYCARBONATE Polycarbonate	Horizontal 90°	100	259 min	1180	14	0.016	27
PAC	PA CF Polyamide With Carbon Fiber	Horizontal 90°	100	259 min	3873	52	0.021	106
PLA	PLA Polylactic acid	Horizontal 90°	100	259 min	2066	52	0.028	62

Properties and characterization of each of the specimens formed in different materials

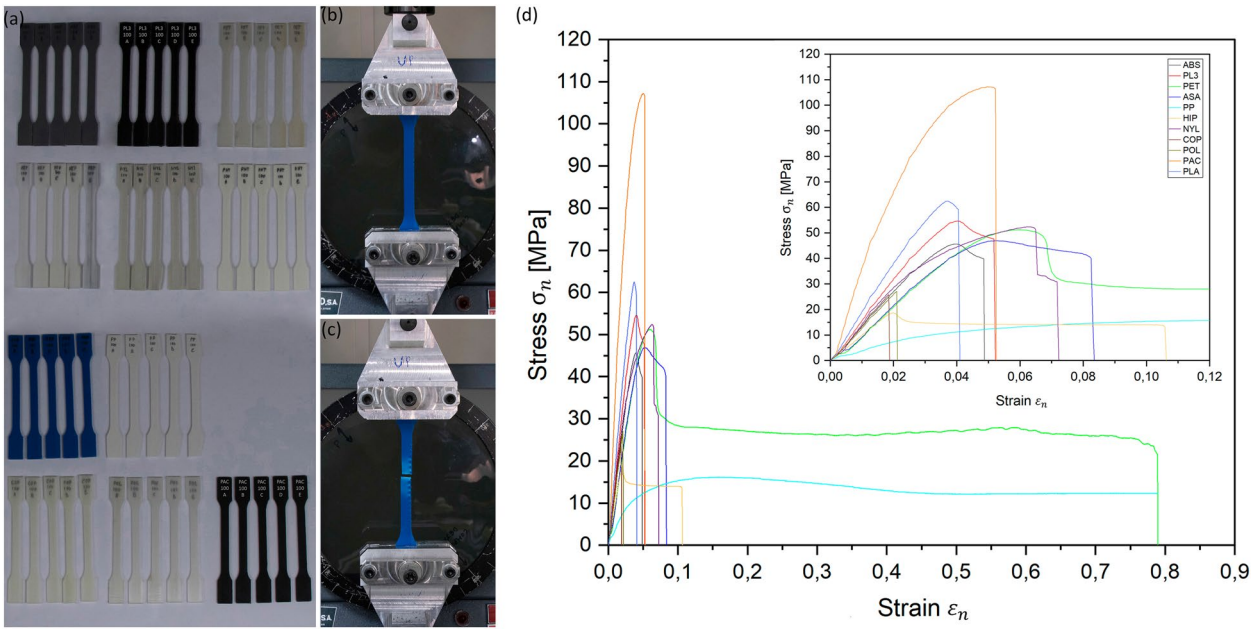

Fig. 10 **a** Tensile specimens of different materials. **b** Before performing tensile tests. **c** After performing tensile tests. **d** Comparison of curves nominal stress $\sigma_n = \frac{F}{A}$ nominal strain $\varepsilon_n = \frac{\Delta L_0}{L_0}$

Table 3 Bending test results of the different specimens tested

Specimens	Printing material	Orientation	Filling density (%)	Printing time per specimen	Bending strain yield strength	Bending modulus [MPa]	Bending stress [MPa]
PH10	PLA Polylactic acid	Horizontal 0°	10	54 min	0.031	2216	80
PH50	PLA Polylactic acid	Horizontal 0°	50	58 min	0.033	2405	86
PH100	PLA Polylactic acid	Horizontal 0°	100	81 min	0.038	2604	107
PHC10	PLA Polylactic acid	Horizontal 90°	10	60 min	0.032	2390	88
PHC50	PLA Polylactic acid	Horizontal 90°	50	62 min	0.030	2664	94
PHC100	PLA Polylactic acid	Horizontal 90°	100	94 min	0.035	2851	117
PV10	PLA Polylactic acid	Vertical 0°	10	71 min	0.024	2347	67
PV50	PLA Polylactic acid	Vertical 0°	50	72 min	0.024	2651	74
PV100	PLA Polylactic acid	Vertical 0°	100	97 min	0.026	2691	81

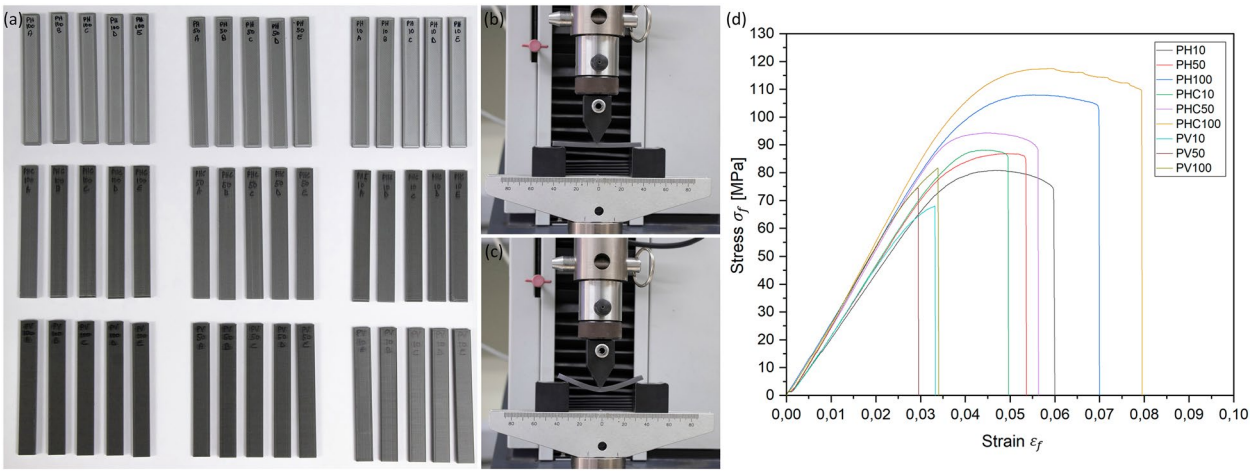

Fig. 11 **a** Three point bending specimens of different PLA positions and densities. **b** Before bending testing. **c** PLA three point bending test process. **d** Comparison of bedning stress $\sigma_f = \frac{3FL}{2bh^2}$ bending deformation $\varepsilon_f = \frac{6sh}{L^2}$

than the expected load that the structures will have to support.

Bending tests: analysis of the printing orientation and filling density of specimens

After conducting three point bending tests, we corroborate that filler density and position play a key role in the mechanical parameters of each specimen. In Table 3 we show the data obtained on the PLA material. In Fig. 11 we present the flexural stress–strain curves in bending.

In Fig. 12 the values of bending modulus versus filling density are ploted. For all geometry an increase in the strength of specimens is observed with the filling density. The same behavior can be shown for the bending stress. It can be observed that the mechanical properties of the specimens at 90° (HOR 90°) are slightly higher than the other ones geometry. Based on these results, the horizontal position at 90° has been chosen for testing the different materials.

Bending tests: analysis of different thermoplastic materials

In the case of bending tests, on Table 4 we show the mechanical properties of the 11 materials analyzed. In Fig. 13, we show how their different flexural stress–strain curves in bending. The highest values can be seen in the PA CF material. However, as mentioned in the previous contribution on the tensile tests, despite its good mechanical performance its values are excessively high for the needs of the study. Moreover, if we take into account the difficulty of printing, this material is to be discarded. The second material with the best mechanical properties was PLA. It has a flexural modulus of

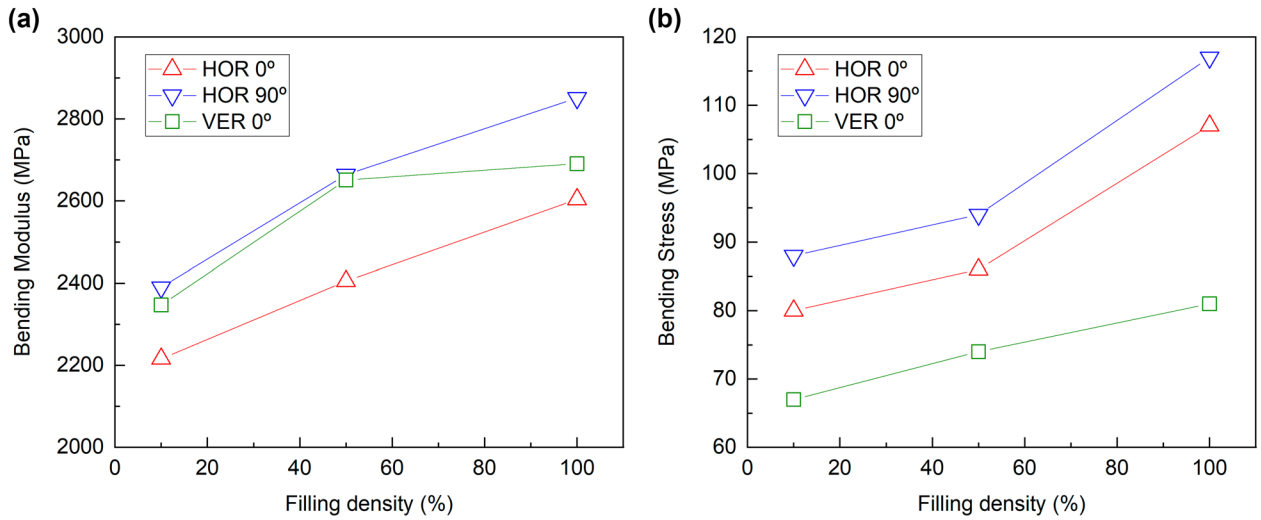

Fig. 12 **a** Relationship between bending modulus and infill density of specimens with different positions. **b** Relationship between bending stress and infill density of specimens with different positions

Table 4 Results of bending tests

Specimens	Printing material	Orientation	Filling density (%)	Printing time per specimen	Bending strain Yield strength	Bending modulus [MPa]	Bending stress [MPa]
ABS	ABS Acrylonitrile Butadiene Styrene	Horizontal 90°	100	91 min	0.038	1823	78
PL3	PLA 3D870 Polylactic acid	Horizontal 90°	100	79 min	0.034	2700	105
PET	PETG Polyethylene Terephthalate	Horizontal 90°	100	79 min	0.041	1793	84
ASA	ASA Acrylonitrile Styrene Acrylate	Horizontal 90°	100	79 min	0.041	1812	77
PP	PP Polypropylene	Horizontal 90°	100	63 min	0.036	689	25
HIP	HIPS Polystyrene and Polybutadiene Rubber	Horizontal 90°	100	79 min	0.022	1375	37
NYL	NYLSTRONG Nylon [PA6] Polyamide With Glass Fiber	Horizontal 90°	100	79 min	0.034	2822	109
COP	INNOVATEFIL CO-POLYESTER Copolyester	Horizontal 90°	100	79 min	0.016	2340	41
POL	INNOVATEFIL POLYCARBONATE Polycarbonate	Horizontal 90°	100	79 min	0.031	2120	87
PAC	PA CF Polyamide With Carbon Fiber	Horizontal 90°	100	79 min	0.032	7076	198
PLA	PLA Polylactic acid	Horizontal 90°	100	79 min	0.035	2851	117

Properties and characterization of each of the specimens formed in different materials

approximately 2850 MPa and a bending stress of 117 MPa equivalent to 1193 kg/cm^2.

Based on the results obtained in both the tensile and bending tests, and taking into account the weight of the fragments to be bonded (little finger 3.08 g, ring finger 7.80 g, the right foot of the fetus 36.20 g, and left hand 223.70 g), we determined that the PLA material has the most appropriate mechanical properties for this case study. Therefore, the various pieces that make up each of the auxiliary structures were printed in a horizontal position at 90° with a filling density of 100%.

3D printing of support structures

The printed parts with the parameters of 0.1 mm in layer height have been more than enough to reproduce the designed virtual models with great quality. The 100% infill density with a grid pattern has endowed the inside of each part with enormous strength. Regarding the applied printing speed of 50 mm/s, it has achieved an optimal layer-to-layer adhesion (Fig. 14).

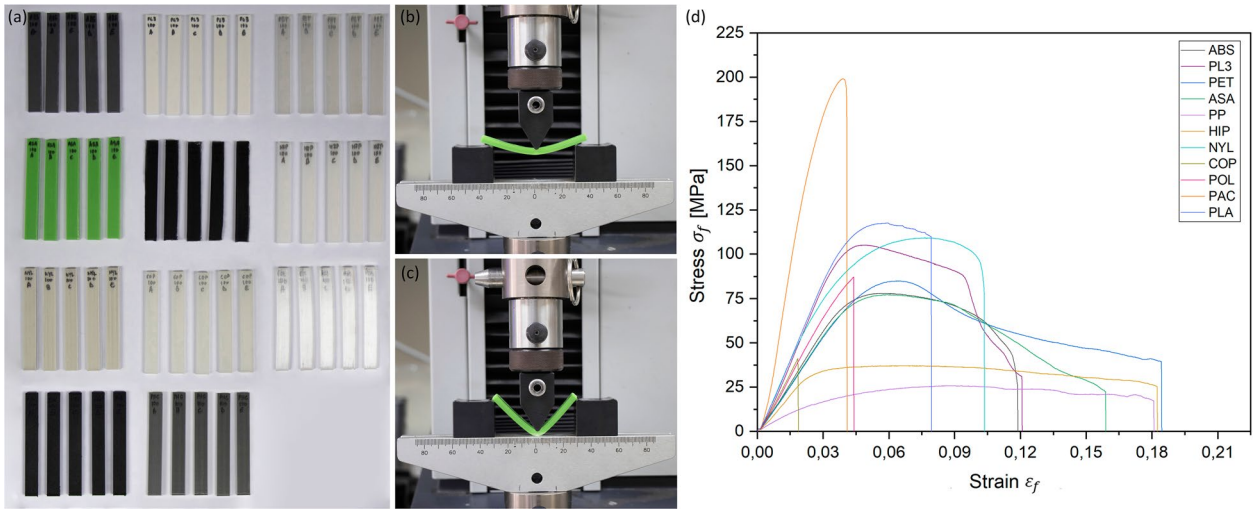

Fig. 13 **a** Flexure specimens of different materials. **b** Before performing the flexure tests. **c** After performing the flexure tests. **d** Comparison of flexural stress curves $\sigma_f = \frac{3FL}{2bh^2}$ flexural strain $\varepsilon_f = \frac{6sh}{L^2}$.

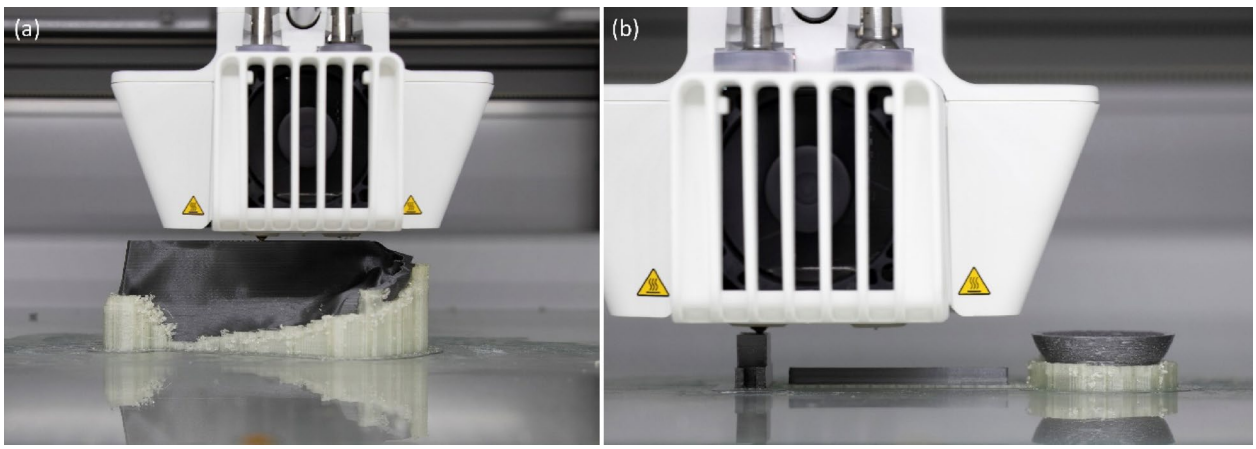

Fig. 14 The printing process of the different pieces that make up the structures. **a** Individual printing of an auxiliary structure in a horizontal position at 45°. **b** Group printing of several elements in a horizontal position at 90°

The use of two extruders during printing offered a high quality with precise finishes in each of the pieces obtained. The PVA material reinforced the most complex points and its subsequent removal has been easily carried out mechanically. The designed system of auxiliary structures composed of the base, clamps with screws and nuts, the set of spheres, the masts that are housed in the spheres, and the auxiliary structure that adapt to the surface of each fragment, have provided an easy, safe, and precise mechanism to stabilize the fragments in the desired positions (Fig. 15).

Application of auxiliary structures for the adhesion of fragments on the anatomical model

As part of the methodological strategy for the curative conservation of mechanical damage, we opted to use 3D printed auxiliary structures that had been specifically designed to support the fragmented elements (hand, fingers and foot). In order to stabilize the fragments and provide them with adequate adhesion, during the first phase we took into account the characteristics of the material, including the weight and position of each fragment. That's why we chose to use the Epo® 155 resin

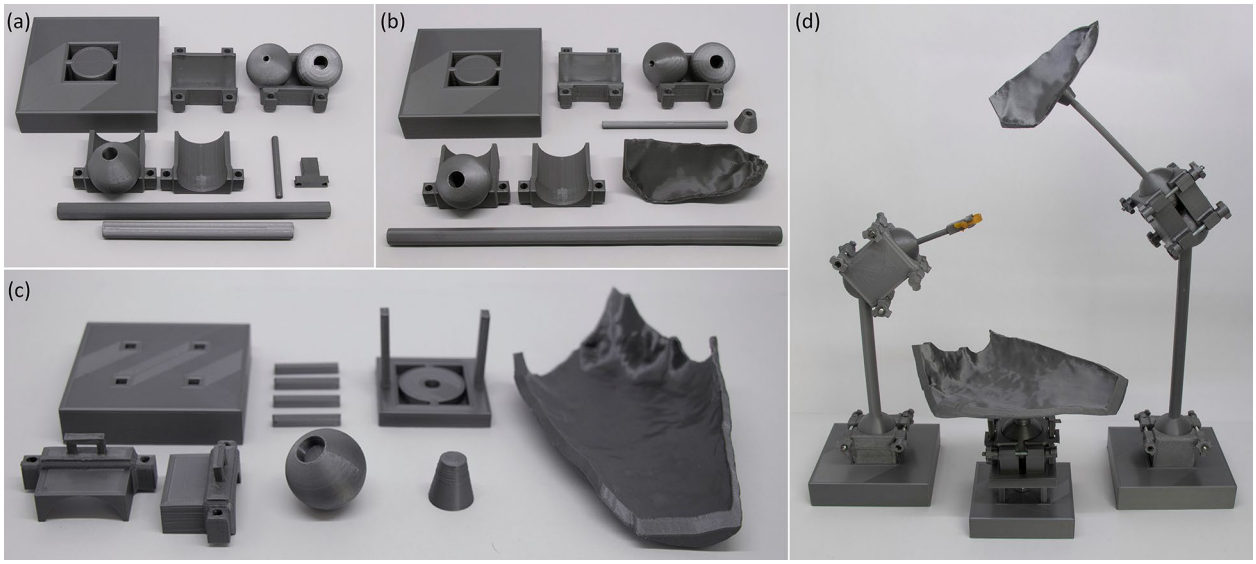

Fig. 15 **a** Structures for adhesion of the fingers. **b** Structures for adhesion of the foot. **c** Structures for adhesion of the hand. **d** Assembled structures

combined with K 156 Hardener, and added 5% Lovel 27 micronized silica [23]. This product, which becomes totally transparent when dry, was selected due to its versatility, optimum mechanical properties of strength and stability, high flexibility and good adhesion. The addition of silica was necessary to give the mixture a slight viscosity in order to better adapt it to the irregularities of the surfaces to be treated. We applied this by injection and brushing. Due to its irregular edges, and to achieve optimum consolidation in the area Lascaux® 443-95, a compound of microcrystalline wax and a synthetic polyterpene resin, was applied to fill the hollow spaces in some of the fragments [24]. Its resin serves as an elastomer that provides excellent adhesive and bonding strength, and improves moisture resistance, wettability, low viscosity, and hot bonding. In the areas of the sculpture to be treated, the previously liquefied product was injected into the hot bath at 60 °C. During the solidification phase, the wax was modeled to adapt it to the shapes with the help of spatulas and dental probes. We considered it essential to allow a period of 48 h to elapse between the application of each layer to ensure complete curing of the product. This operation was repeated until the desired level of filling was achieved.

The adhesion process corresponding to the hand turned out to be somewhat complex due to the fact that the metal bolt preserved in the work no longer had its original position. This is a result of inadequate manipulations and previous poorly executed interventions. During this preliminary phase, the virtual anastylosis studies have proved to be an extremely valuable tool to determine the ideal position of each fragment.

The 3D printed auxiliary structure that holds the obstetrician's hand has been perfectly adapted to the volume of the hand with millimeter precision. This provided a precise fit and thus a high degree of stability in the established position. The elevation system of the clamp with the sphere inside allowed millimeter-scale movements in the adjustment of the orientation (Fig. 16a). This made it possible to place the fragment in its original position. The adhesion was conducted by applying the resin at key points including on the metal pin and the wax in areas close to it. Due to the enormous loss of waxy material in the damaged areas, once the adhesion was completed, the hand have not completely stable (Fig. 16b). To solve this problem and to guarantee the required strength in the damaged area, we volumetrically reintegrated the hollow spaces with the wax paste (Fig. 16c and d). After 48 h, the wax paste solidified correctly providing the area with great strength, and completely stabilizing the fragment. The application of the wax by injection made it possible to access all the spaces, achieving a firm and resistant adhesion.

Regarding the intervention on the foot, it turned out to be less complex than in the previous case. The auxiliary structure of the structure, which gathers and holds this anatomical part of the sculpture by its sole, was completely adapted to the shape of the fragment (Fig. 17a). The set of elements that make up the structure made it possible to locate the exact original position of the limb with great precision. The fragment was attached using

Fig. 16 Adhesion process of the fragments using the 3D printed auxiliary structures. **a** Adjustment of the auxiliary structure to place the hand in its original location. **b** Missing material between the hand and the work. **c** Injection of the new wax to volumetrically reintegrate the losses. **d** Modeling of the volumetric reintegration

the original metal rod that was preserved. Due to the non-uniform edges between the joints, once this process was completed the hollow spaces were reintegrated volumetrically with wax. Regarding the middle and ring fingers, we chose to insert a small 20 mm fiberglass rod to guarantee their stability once they have adhered to the work as a whole. The small dimensions of the little finger did not require any additional reinforcement. During the adhesion we placed each element in its exact position thanks to the auxiliary structures and to the different heads on whose extremities elastic bands were placed to hold each one of the fingers (Fig. 17b–d).

In the five adhesions conducted with the aid of the auxiliary structures, the process proved to be very effective. We achieved great stability, resistance, safety, and precision in each of the treatments applied to the sculpture (Fig. 18).

Conclusion

3D digitization using structured light scanners has proven to be an effective tool when conservator-restorers need a high-precision, high-resolution model on which to study different intervention alternatives. The analysis of each of the treatments carried out using virtual anastylosis has made it possible to study in detail the necessary designs of the auxiliary structures through digital modeling. The precision established in the auxiliary structures was perfectly reproduced during 3D printing, adapting exactly to the fragments that make up the work.

The analysis of mechanical behavior conducted by tensile and bending testing show that *FDM* thermoplastic printing materials are strongly dependent with the geometry pattern used to build the specimen. An induced anisotropy is then present in the specimens by the building method. The relative orientation of filaments formed during printing process is very important to get the best mechanical properties of specimens. Specimens with filaments oriented along applied tensile have the best behavior. The PLA filament determined that specimens

Fig. 17 Adhesion process of the fragments using the 3D printed auxiliary structures. **a** Adhesion process of the foot. **b**–**d** Adhesion process of the toes

Fig. 18 **a** Initial state of the work before the intervention. **b** Current state after the intervention

oriented with a 90° horizontal position at 100% filler density were the strongest. Among the various types of materials characterized, PLA also proved to be the most suitable due to its good mechanical performance and easy printing process. The set of structures applied during the adhesion of fragments proved to be a great alternative to conventional systems. The methodology developed under the criterion of minimum intervention was respected

at all times. Because of it, manipulations during treatments were considerably reduced and the intervention ensured with maximum precision, safety and rigor. The tools used in this research can be of great help to professionals in the field of conservation and restoration of cultural heritage. However, when performing adhesions of complex fragments, the approach methods must be adjusted to the characteristics of each specific work. This includes taking into consideration the weight of the work and fragments, the angles of union, the volumetric complexity, the constituent material of the work, and the 3D printing material. Finally, one must pay attention to the orientation of the printing of each of the pieces that make up the structures.

Abbreviations

FDM: Fused deposition modeling; ABS: Acrylonitrile butadiene styrene; PETG: Polyethylene terephthalate; ASA: Acrylonitrile styrene acrylate; NYLSTRONG: Nylon [PA6] polyamide with glass fiber; HIPS: Polystyrene and polybutadiene rubber; INNOVATEFIL POLYCARBONATE: Polycarbonate; PP: Polypropylene; PLA: Polylactic acid; PLA 3D870: Polylactic acid; INNOVATEFIL CO-POLYESTER: Copolyester; PA CF: Polyamide with carbon fiber; PVA: Polyvinyl alcohol; ISO: International Organization for Standardization; STL: Standard template library.

Acknowledgements

The authors would especially like to thank Fermín Viejo Tirado, director of the Javier Puerta Anatomy Museum of the Faculty of Medicine (UCM), and Carlos Romero Izquierdo, technician of the Department of Materials Physics of the Faculty of Physical Sciences (UCM), for their collaboration.

Author contributions

ESM conceptualization. ESM, ÓHM and ASO methodology. ÓHM 3D digitization and virtual reconstruction. ESM digital modeling and 3D printing. ESM mechanical testing. ESM and JRE interpretation of mechanical test data. ESM and ASO intervention in the real work. ASO and ÓHM funding acquisition. ESM writing—original draft. ESM, ÓHM, JRE and ASO writing—revising and editing. All authors read and approved the final manuscript.

Funding

This work is funded by the Ministry of Science, Innovation and Universities (Spain) within the State Program of Knowledge Generation and Scientific and Technological Strengthening R&D+i, State Subprogram of Knowledge Generation, through the research project Ref.: PGC2018-098396-B-100 Innovative methodologies in conservation-restoration of scientific collections with didactic models of botany, human and animal anatomy based on 3D technologies, and thanks to the funds of the FPI Predoctoral Fellowship ref.PRE2019-087870 financed by the Ministry of Science and Innovation (Spain), FSE European Social Fund and the State Research Agency.

Availability of data and materials

Not applicable.

Declarations

Ethics approval and consent to participate

Not applicable.

Consent for publication

Not applicable.

Competing interests

The authors declare that they have no competing interests.

Author details

[1]Department of Painting and Conservation-Restoration, Faculty of Fine Arts, Complutense University of Madrid, C/ Pintor el Greco, 2. Ciudad Universitaria s/n, 28040 Madrid, Spain. [2]Department of Design and Image, Faculty of Fine Arts, Complutense University of Madrid, C/ Pintor el Greco, 2. Ciudad Universitaria s/n, 28040 Madrid, Spain. [3]Department of Physics of Materials, Faculty of Physical Sciences, Complutense University of Madrid, Plaza Ciencias, 1. Ciudad Universitaria s/n, 28040 Madrid, Spain.

Received: 8 April 2022 Accepted: 14 June 2022
Published online: 07 July 2022

References

1. Bonells J, Lacaba I. Curso completo de anatomía del cuerpo humano, vol. V. en Madrid: en la imprenta de Sancha; 1800.
2. Sánchez Ortiz A, Matia Martín P. Modelos plásticos o simulacros de carne. Procedimientos tecnológicos en la creación de esculturas en cera. De Arte. 2016;15:310–26.
3. Sánchez Ortiz A. Restauración de modelos anatómicos en cera: colección del Real Colegio de Cirugía de San Carlos. Ge-Conservacion. 2015;7:37–49. https://doi.org/10.37558/gec.v7i0.274.
4. Riccardelli C, Morris M, Wheeler G, Soultanian J, Becker L, Street, R. The treatment of Tullio Lombardo's Adam: a new approach to the conservation of monumental marble sculpture. Metrop Mus J. 2014;49:49–116. http://www.metmuseum.org/-/media/Files/Exhibitions/2014/Journal49_Riccardelli_pp048-116.pdf. Accessed 18 Oct 2021.
5. Van Damme T, Auer J, Ditta M, Grabowski M, Couwenberg M. The 3D annotated scans method: a new approach to ship timber recording. Herit Sci. 2020;8:75. https://doi.org/10.1186/s40494-020-00417-9.
6. Jo YH, Hong S, Jo SY, Kwon YM. Noncontact restoration of missing parts of stone Buddha statue based on three-dimensional virtual modeling and assembly simulation. Herit Sci. 2020;8:103. https://doi.org/10.1186/s40494-020-00450-8.
7. Carvalho M, Debut V, Antunes J. Physical modelling techniques for the dynamical characterization and sound synthesis of historical bells. Herit Sci. 2021;9:157. https://doi.org/10.1186/s40494-021-00620-2.
8. Sánchez Ortiz A, Hernández-Muñoz Ó, Sterp Moga E. Flora Artefacta. Historia, Tecnología y Conservación de la Colección de Modelos Botánicos Brendel en la Universidad Complutense de Madrid. An Hist Arte. 2021;31:103–25. https://doi.org/10.5209/anha.78052.
9. Sterp Moga E, Hernández-Muñoz Ó, Sánchez-Ortiz A. Application of light sources on photogrammetric models for the diagnosis and virtual restoration of objects in polychrome wax. Conservar Património. 2021;38:10–21. https://doi.org/10.14568/cp2020021.
10. Byron CD, Kiefer AM, Thomas J, Patel S, Jenkins A, Fratino AL, Anderson T. The authentication and repatriation of a ceremonial tsantsa to its country of origin. Herit Sci. 2021;9:50. https://doi.org/10.1186/s40494-021-00518-z.
11. Balletti C, Ballarian M, Guerra F. 3D printing: state of the art and future perspectives. J Cult Herit. 2017;26:172–82. https://doi.org/10.1016/j.culher.2017.02.010.
12. Jo YH, Hong S. Application of three-dimensional scanning, haptic modeling, and printing technologies for restoring damaged artifacts. J Conserv Sci. 2019;35(1):71–80. https://doi.org/10.12654/jcs.2019.35.1.08.
13. Hernández-Muñoz Ó, Aranda Gabrielli D, Maruri Palacín A, Sterp Moga E, Sánchez-Ortiz A. 3D digital technologies for the elaboration of a replica of a dermatological didactic model belonging to the olavide museum from the original mould. Heritage. 2022;5:702–15. https://doi.org/10.3390/heritage5020039.
14. Belter JT, Dollar AM. Strengthening of 3D printed fused deposition manufactured parts using the fill compositing technique. PLoS ONE. 2015;10:4. https://doi.org/10.1371/journal.pone.0122915.
15. Doungkom P, Jiamjiroch K. Analysis of printing pattern and infiltration percent over the tensile properties of PLA printed parts by a fuse deposition modelling printer. IOP Conf Series Mater Sci Eng. 2019. https://doi.org/10.1088/1757-899X/501/1/012028.
16. Soud WA, Baqer IA, Ahmed MR. Experimental study of 3D printing density effects on the mechanical properties of the carbon-fiber and polylactic

acid specimens. Eng Technol J. 2019;37(4A):128–32. https://doi.org/10.30684/etj.37.4A.3.
17. Andó M, Birosz M, Jeganmohan S. Surface bonding of additive manufactured parts from multi-colored PLA materials. Measurement. 2021. https://doi.org/10.1016/j.measurement.2020.108583.
18. Chen J, Liu X, Tian Y, Zhu W, Yan C, Shi Y, Kong LB, Qi HJ, Zhou K. 3D-printed anisotropic polymer materials for functional applications. Adv Mater. 2021. https://doi.org/10.1002/ADMA.202102877.
19. Torrado AR, Shemleya CM, English JD, Lin Y, Wicker RB, Roberson DA. Characterizing the effect of additives to ABS on the mechanical property anisotropy of specimens fabricated by material extrusion 3D printing. Addit Manuf. 2015;6:16–29. https://doi.org/10.1016/j.addma.2015.02.001.
20. Torrado Perez AR, Roberson DA, Wicker RB. Fracture surface analysis of 3D-printed tensile specimens of novel ABS-based materials. J Fail Anal Prev. 2014;14:343–53. https://doi.org/10.1007/s11668-014-9803-9.
21. Buchwald MD, Breed MD, Greenberg AR. The thermal properties of beeswaxes: unexpected findings. J Exp Biol. 2008;211(1):121–7.
22. Gabbriellini C, Nesi G, Rossi F, Santi R, Speranza L. La collezione di cere del Museo di Anatomia Patologica di Firenze. Note sulle vicende storiche, sulla técnica esecutiva e sui restauri. OPD Restauro. 2009;21:51–70.
23. Gabbriellini C, Pradier I, Rossi F, Rossignoli G, Dallatana D, Porro A, Speranza L, Toni R. Il restauro dello Spellato del Museo dipartimentale S.Bi.Bi.T. dell'Università di Parma Biomateriali e tecnologie innovative per la valorizzazione della ceroplastica settecentesca. OPD Restauro. 2013;25:37–52.
24. Hierl C. Untersuchung und Konservierung des Materialbildes Sonne von Michael Buthe. Unpublished diploma thesis. University of Applied Arts. 2000.

Publisher's Note